

## Supporting Information

Flash time / s →	0	0.2	0.4	0.6	0.8	1.0	1.2	1.4	1.6	1.8	2.0	2.2	2.4	2.6	2.8	3.0	3.2	3.4	3.6
Chem. composition	Sample number																		
<b>FA<sub>0.8</sub>CsxMA<sub>0.2-X</sub></b>																			
X=0	1	2	3	4	5	6	7	8	9	10	11	12	13	14	15	16	17	18	19
X=0.05	20	21	22	23	24	25	26	27	28	29	30	31	32	33	34	35	36	37	38
X=0.1	39	40	41	42	43	44	45	46	47	48	49	50	51	52	53	54	55	56	57
X=0.15	58	59	60	61	62	63	64	65	66	67	68	69	70	71	72	73	74	75	76
X=0.2	77	78	79	80	81	82	83	84	85	86	87	88	89	90	91	92	93	94	95
<b>FA<sub>0.85</sub>CsxMA<sub>0.15-X</sub></b>																			
X=0	96	97	98	99	100	101	102	103	104	105	106	107	108	109	110	111	112	113	114
X=0.05	115	116	117	118	119	120	121	122	123	124	125	126	127	128	129	130	131	132	133
X=0.1	134	135	136	137	138	139	140	141	142	143	144	145	146	147	148	149	150	151	152
X=0.15	153	154	155	156	157	158	159	160	161	162	163	164	165	166	167	168	169	170	171
<b>FA<sub>0.9</sub>CsxMA<sub>0.1-X</sub></b>																			
X=0	172	173	174	175	176	177	178	179	180	181	182	183	184	185	186	187	188	189	190
X=0.05	191	192	193	194	195	196	197	198	199	200	201	202	203	204	205	206	207	208	209
X=0.1	210	211	212	213	214	215	216	217	218	219	220	221	222	223	224	225	226	227	228
<b>FA<sub>0.95</sub>CsxMA<sub>0.05-X</sub></b>																			
X=0	229	230	231	232	233	234	235	236	237	238	239	240	241	242	243	244	245	246	247
X=0.05	248	249	250	251	252	253	254	255	256	257	258	259	260	261	262	263	264	265	266

Table S1. Sample chemical compositions and flash times.

Sample	Displ .	a_displfix	c_displ_fix	ratio_axe s displ fix	V_displ_fix	a-axis	error_a	c-axis	error_c	ratio_axe s displ free	V_displ_free	Comments
Vario system	free	to -0.0238	to -0.0238									simple axial and initial displacement refined on <b>FA<sub>0.8</sub>MA<sub>0.05</sub>Cs<sub>0.15</sub>PbI<sub>3</sub></b> Vario to -0.0238, fixed then consecutively
FA <sub>0.8</sub> MA <sub>0.15</sub> Cs <sub>0.05</sub> PbI <sub>3</sub>	-0.0169	8.9659	12.6152	1.40702	113.10662	8.9641	4E-4	12.6126	0.001	1.40701	113.34941	Strong peak at 12 2Theta
FA <sub>0.8</sub> MA <sub>0.1</sub> Cs <sub>0.1</sub> PbI <sub>3</sub>	0.0151	8.9546	12.6571	1.41347	113.33927	8.9489	3E-4	12.6405	0.001	1.41252	113.11857	Nearly pure 3D, impurity at 12 2Theta
FA <sub>0.8</sub> MA <sub>0.05</sub> Cs <sub>0.15</sub> PbI <sub>3</sub>	-0.0238	--	--	--	--	8.9211	3E-4	12.5988	0.001	1.41225	112.39515	Nearly pure 3D Pv, some impurity peaks, bad fit 022: calc pos < obs pos
FA <sub>0.8</sub> Cs <sub>0.2</sub> PbI <sub>3</sub>	-0.0416	8.9333	12.6883	1.42034	113.34839	8.9362	5E-4	12.6932	7E-4	1.42042	113.42897	Peaks splitting, e.g. 14 24 (022) and 28
FA <sub>0.85</sub> MA <sub>0.1</sub> Cs <sub>0.05</sub> PbI <sub>3</sub>	-0.0214	8.9342	12.6583	1.41684	113.09178	8.9338	3E-4	12.6576	5E-4	1.41682	113.08047	Nearly pure 3D, good fit on (022), very small impurities
FA <sub>0.85</sub> MA <sub>0.05</sub> Cs <sub>0.1</sub> PbI <sub>3</sub>	-0.0259	8.9251	12.6429	1.41656	112.83915	8.9253	3E-4	12.6434	5E-4	1.41658	112.84614	Pure 3D, no impurities
FA <sub>0.85</sub> Cs <sub>0.15</sub> PbI <sub>3</sub>	-0.0274	8.9131	12.6367	1.41777	112.63217	8.9133	3E-4	12.6371	6E-4	1.41778	112.63826	Very pure sample, very minor amount PbI <sub>2</sub>
FA <sub>0.9</sub> MA <sub>0.05</sub> Cs <sub>0.05</sub> PbI <sub>3</sub>	-0.0511	8.9625	12.6341	1.40966	113.23312	8.9675	5E-4	12.6341	0.001	1.40888	113.29629	Nearly pure 3D, (022) well fit but slightly too sharp on calc side
FA <sub>0.9</sub> Cs <sub>0.1</sub> PbI <sub>3</sub>	-0.0495	8.9475	12.6162	1.41003	112.88345	8.9519	5E-4	12.6181	0.001	1.40954	112.95597	Pure 3D with very minor impurity
FA <sub>0.95</sub> Cs <sub>0.05</sub> PbI <sub>3</sub>	-0.051	8.9644	12.6469	1.41079	113.37187	8.9709	4E-4	12.6495	0.001	1.41006	113.4774	Pure 3D with very minor impurity

Table S2. Lattice parameters of the 14 optimal perovskite films by fixing the sample with stoichiometry FA<sub>0.8</sub>MA<sub>0.05</sub>Cs<sub>0.15</sub>PbI<sub>3</sub>.

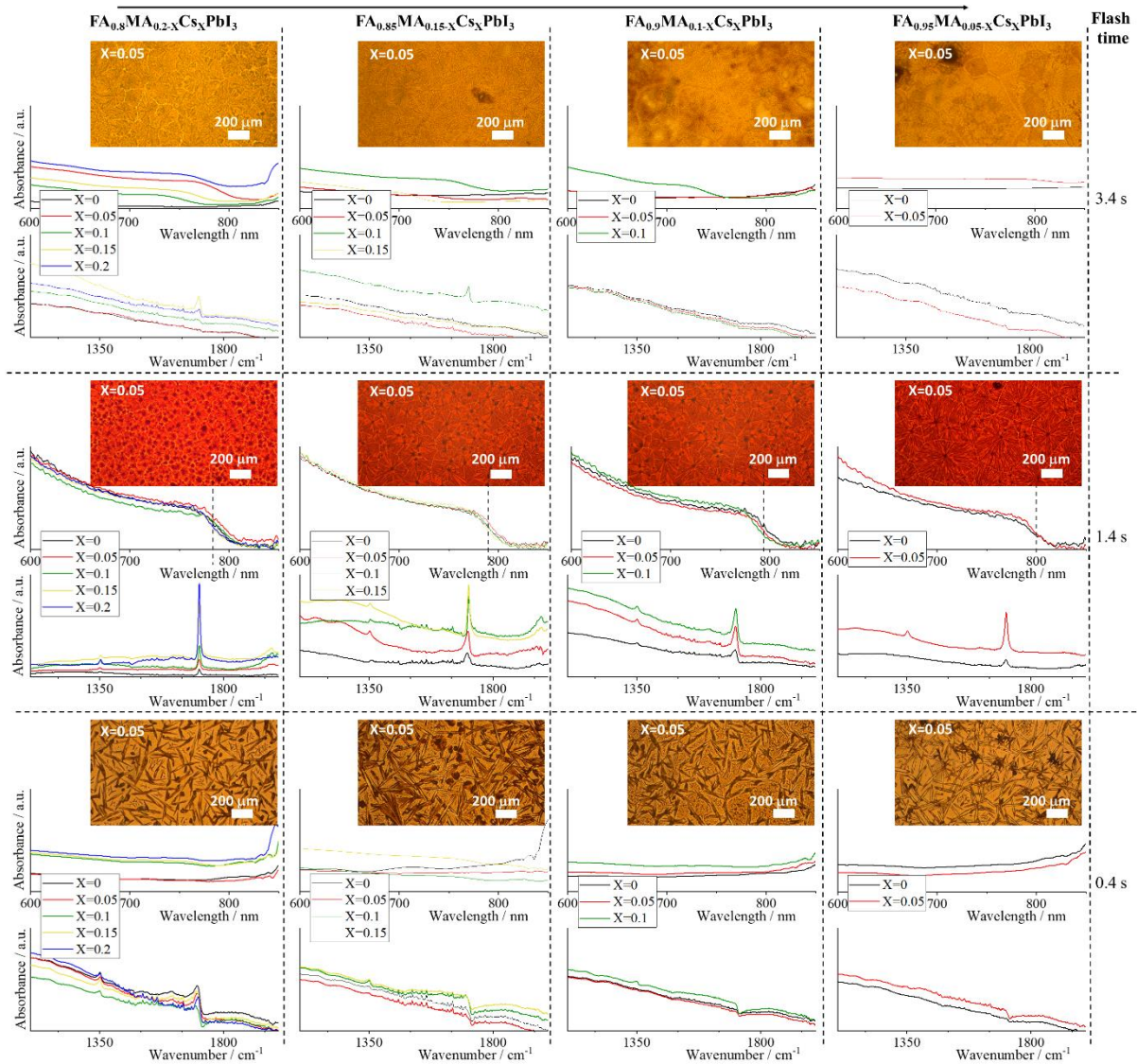


Figure S1. Film evolution during annealing. Optical images in transmission mode, optical absorption spectra, and FTIR measurement were performed in a chosen film spot for four perovskite compositions and three flash times.

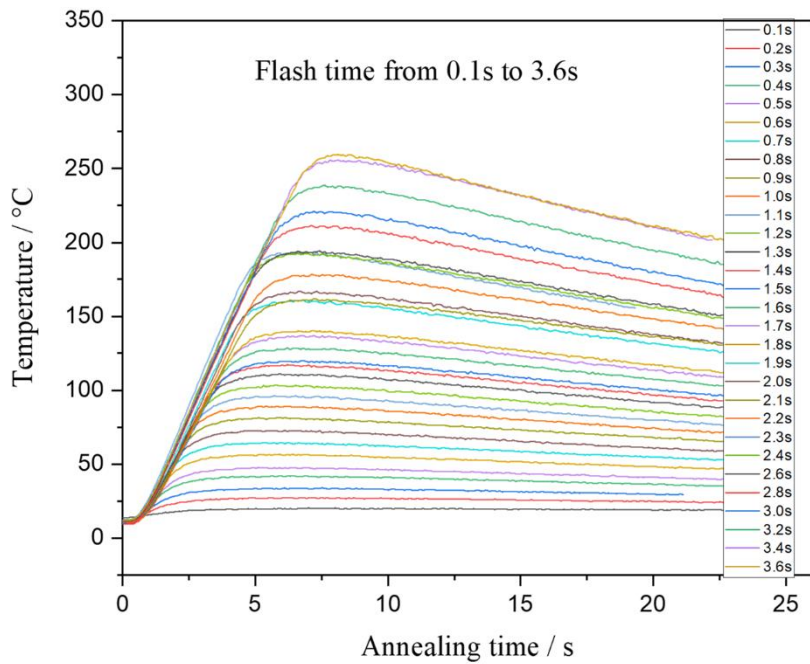


Figure S2. Temperate profile as a function of the annealing time for FIRA processing.

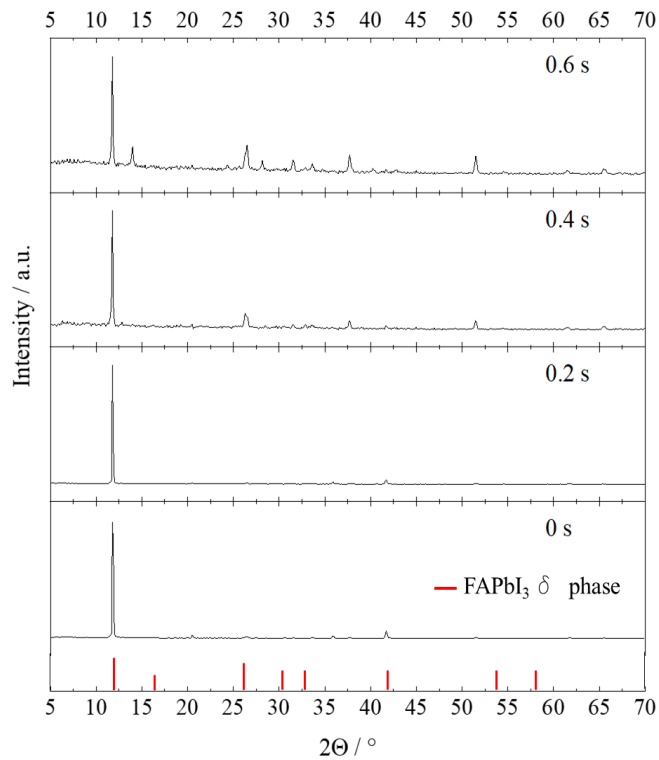


Figure S3. XRD patterns for different annealing time of the  $\text{FA}_{0.85}\text{MA}_{0.1}\text{Cs}_{0.05}\text{PbI}_3$  sample, compared to the reference peaks position of  $\text{FAPbI}_3$   $\delta$  phase.

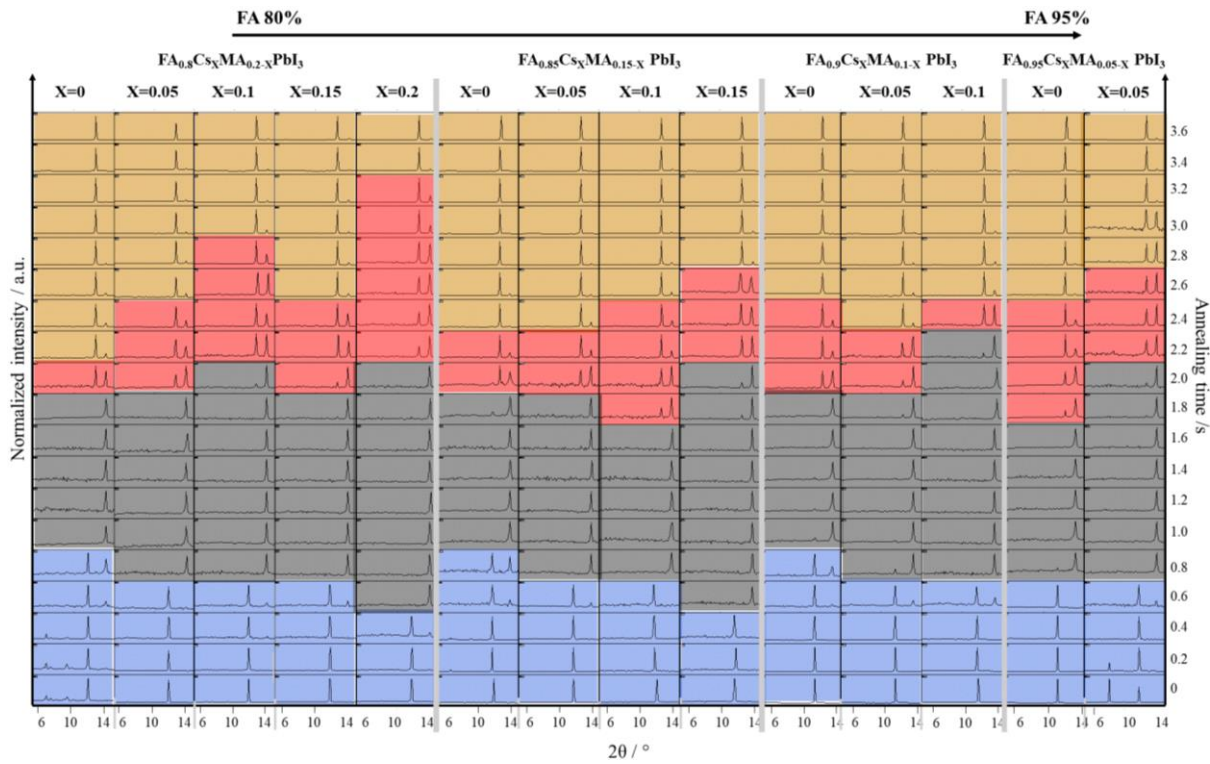


Figure S4. XRD patterns limited from  $2\theta$   $5^\circ$  to  $14^\circ$  for all processed films.

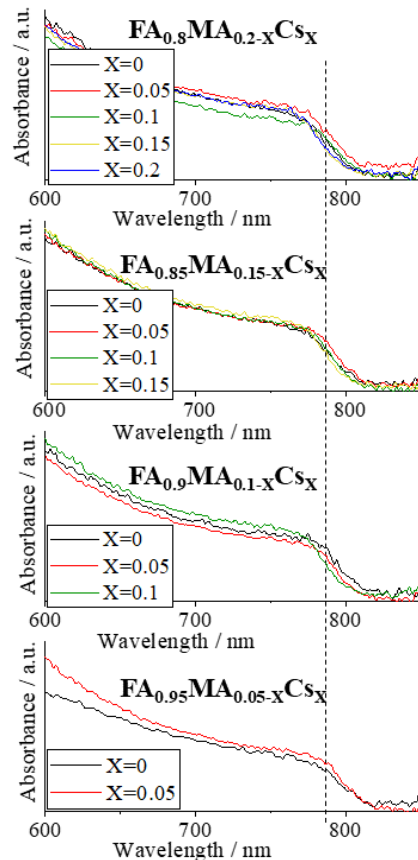


Figure S5. Absorbance spectra for each composition at the determined optimal flash time of 1.4 s.

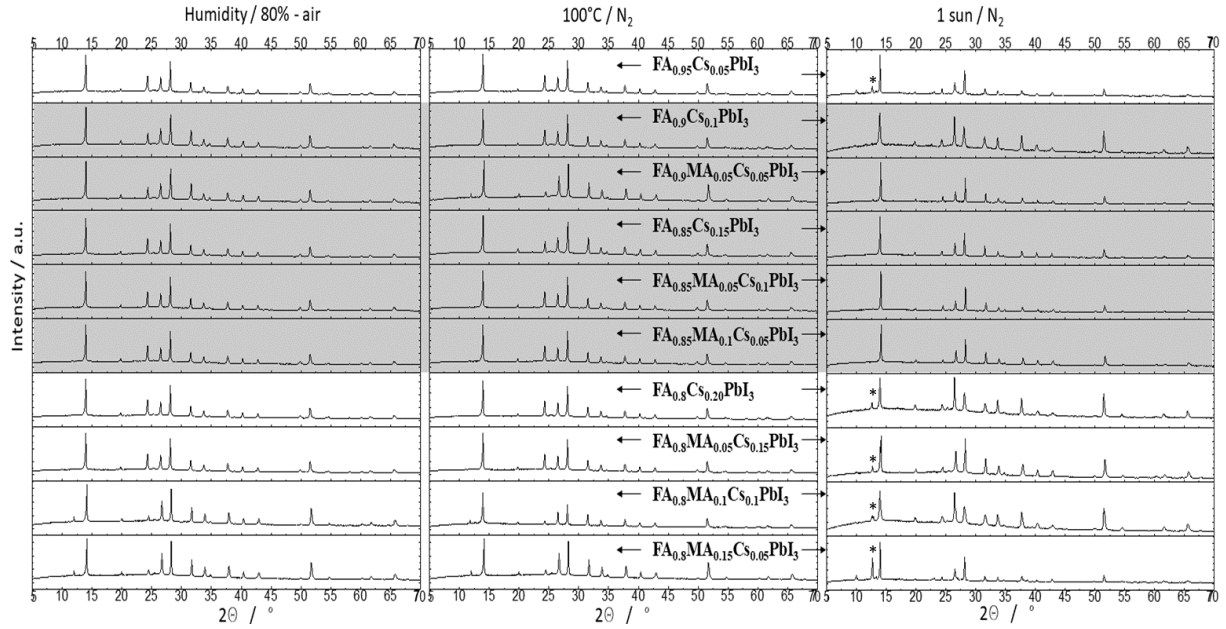


Figure S6. XRD pattern of the stressed ten selected films. The shadowed frames represent the most stable compositions (the marked Bragg reflection with an asterisk denotes the presence of  $\text{PbI}_2$  phase).

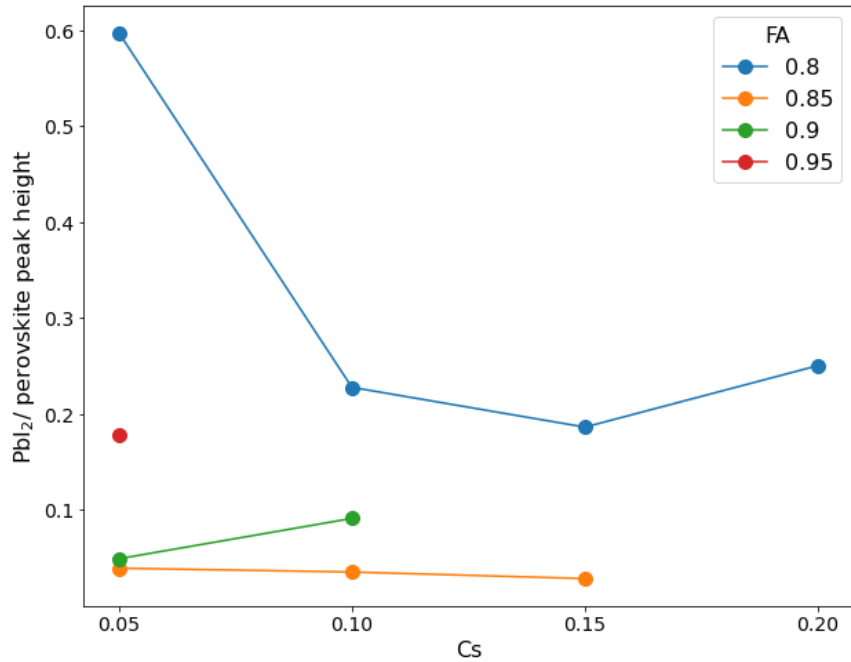


Figure S7. Degradation evolution within each  $FA$  group. Y-axis shows the relative fraction of  $\text{PbI}_2$  to the perovskite phase.

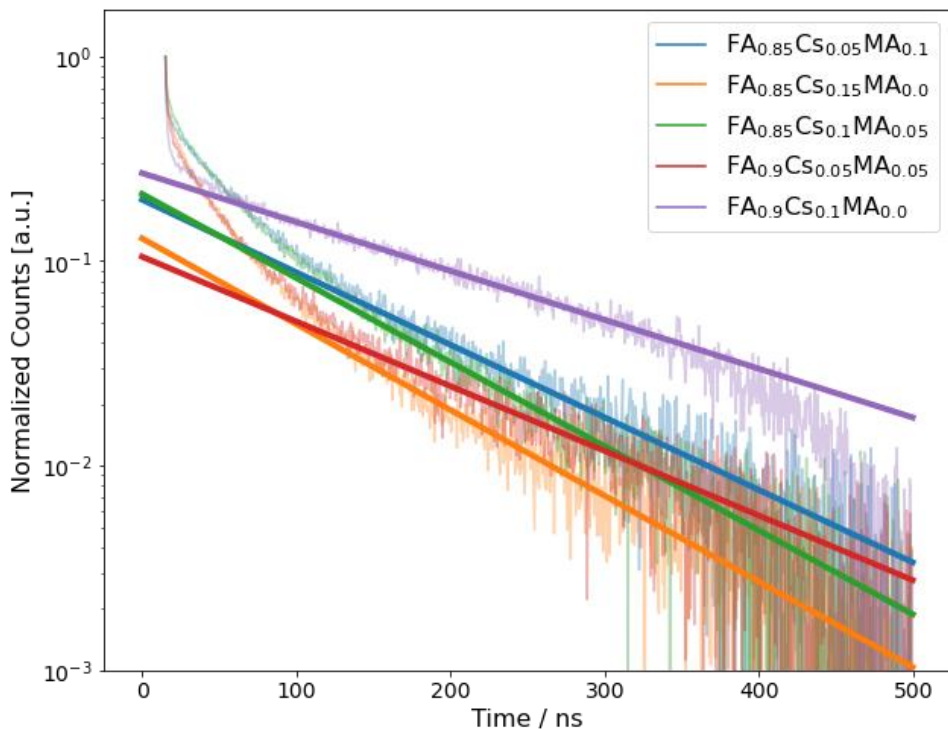


Figure S8. Time resolved PL (TRPL) analysis for the five most stable compositions using a mono-exponential fitting and with an architecture of TCO / m-TiO<sub>2</sub> (150nm, +5) / Perovskite (500nm, +12) / Spiro-OMeTAD (80nm, +4).

The traces show two different features: an initial rapid drop during the first few nanoseconds followed by a slower decrease eventually ending up into a nearly mono-exponential decay. Note that carrier diffusion after the initial exponential excitation profile leads to a concentration equilibration and has no effect on the TRPL traces at the time-scale shown here.<sup>98</sup> In addition, with the low laser fluences used here (5 nJ/cm<sup>2</sup>) radiative and Auger recombination are negligible.<sup>99</sup> Therefore, the initial drop can be attributed to electron transfer from perovskite into TiO<sub>2</sub>, which continues until the quasi-Fermi levels for electrons in the perovskite layer and in the TiO<sub>2</sub> film equilibrate.<sup>100</sup> This equilibration reduces the PL signal by a small amount, which indicates that most carriers remain in the perovskite layer. After this initial electron transfer, the main process is charge carrier recombination in the bulk and at the perovskite/TiO<sub>2</sub> interface which can be described by a monoexponential effective Shockley-Reed-Hall (SRH) recombination with the SRH lifetime  $\tau_{SRH}^{eff}$  (*being*  $\tau_{SRH}^{eff}$  the lifetime of the monoexponential decay).<sup>100</sup>

Cation composition	FA <sub>0.85</sub> Cs <sub>0.05</sub> MA <sub>0.1</sub>	FA <sub>0.85</sub> Cs <sub>0.1</sub> MA <sub>0.0</sub>	FA <sub>0.85</sub> Cs <sub>0.1</sub>	FA <sub>0.9</sub> Cs <sub>0.05</sub> MA <sub>0.0</sub>	FA <sub>0.9</sub> Cs <sub>0.1</sub>
Lifetime / ns	122.39	103.54	105.60	137.24	181.66

Tables S3. Lifetime extracted from the mono-exponential fitting of the TRPL curves.

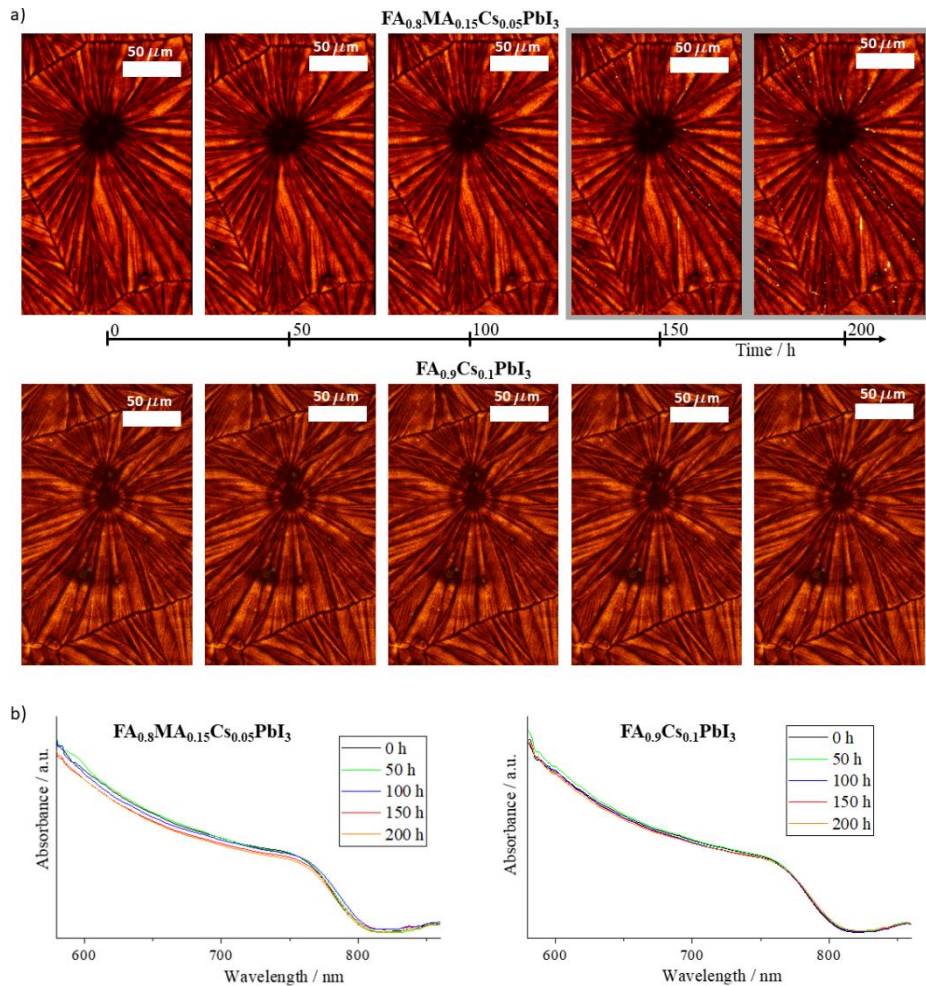


Figure S9. a) Optical image and b) optical absorption spectra of the multication perovskite halide films subjected to 1-sun light and ambient conditions (50% relative humidity, 25°C) for 200h. The shaded rectangle denotes degraded films.



Figure S10. Photograph taken with a thermal camera to measure the surface temperature of the studied film under simulated sunlight (1 sun 1.5AM, Xenon lamp). The central peephole indicates the surface temperature of the perovskite film.

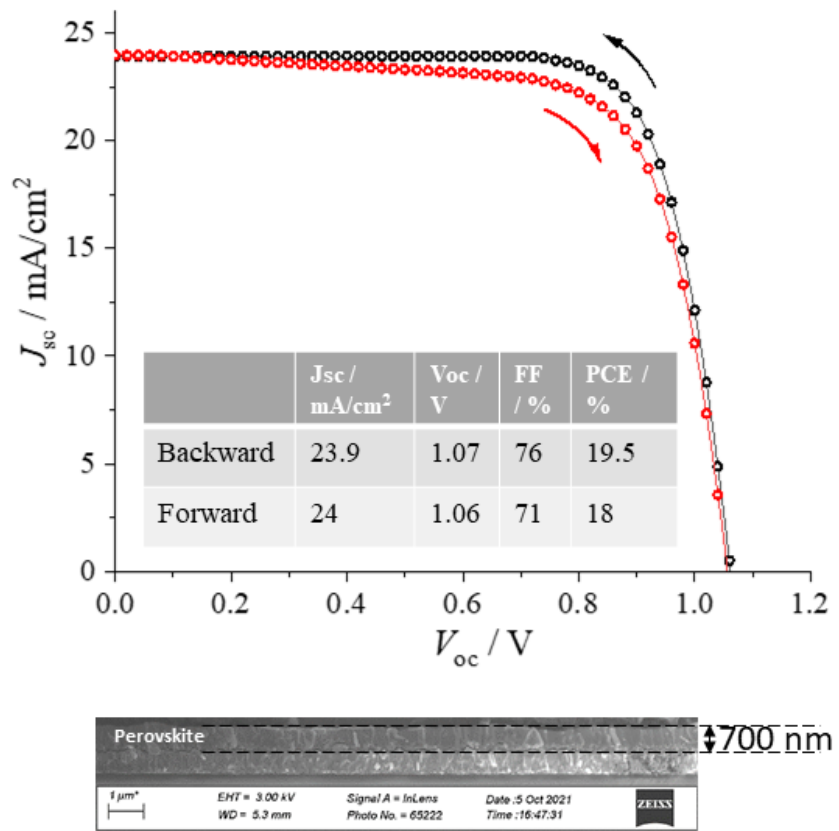


Figure S11. Figure S12. JV scan of the champion cell made at 1.5AM 1sun simulation. The architecture of the cell is composed by FTO / TiO<sub>2</sub> compact-meso / FA<sub>0.9</sub>Cs<sub>0.1</sub>PbI<sub>3</sub>/ Spiro-Ometad / Au. Bottom, refers to the cross-sectional scanning electron microscope image of the cell.

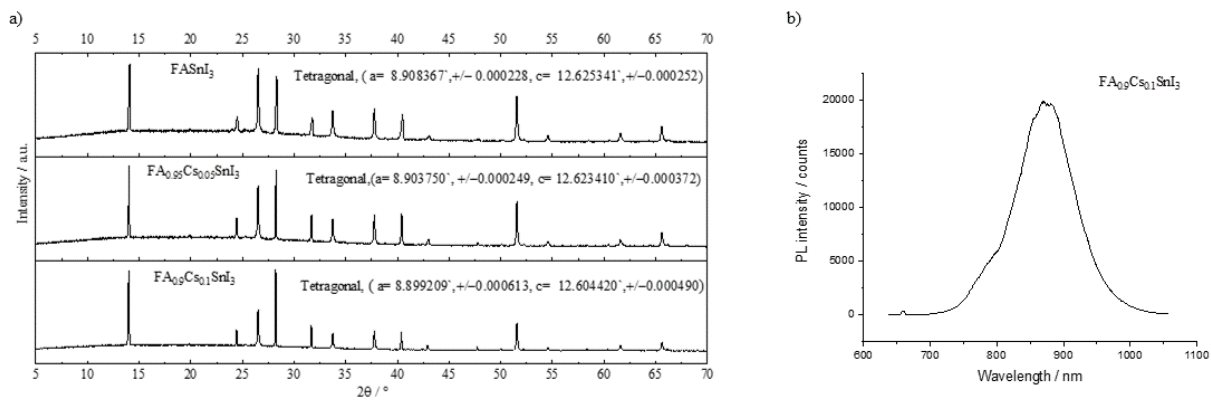


Figure S12. a) XRD patterns of the Sn-based perovskite compositions and its respective fitted lattice parameters. b) Photoluminescence spectrum of the selected Sn based perovskite composition.

Datasets availability: { <https://doi.org/10.5281/zenodo.4907012> }

## References

98. Noel, N. K. *et al.* Highly crystalline methylammonium lead tribromide perovskite films for efficient photovoltaic devices. *ACS Energy Lett.* **3**, 1233–1240 (2018).
99. Kirchartz, T., Márquez, J. A., Stolterfoht, M. & Unold, T. Photoluminescence-based characterization of Halide perovskites for photovoltaics. *Adv. Energy Mater.* **10**, 1904134 (2020).
100. Krückemeier, L., Krogmeier, B., Liu, Z., Rau, U. & Kirchartz, T. Understanding transient photoluminescence in Halide perovskite layer stacks and solar cells. *Adv. Energy Mater.* **11**, 2003489 (2021).